Time-focused crystal analyzer spectrometer†

John M. Carpenter[a] and Géza Zsigmond[b]

[a] Intense Pulsed Neutron Source, Argonne National Laboratory, Argonne, IL 60439, USA.
  E-mail: jmcarpenter@anl.gov; Fax: +1 (630) 252 4263; Tel: +1 (630) 252 5519
[b] Laboratory for Neutron Scattering ETHZ & PSI, CH-5232 Villigen, Switzerland.
  E-mail: geza.zsigmond@psi.ch; Fax: +41 (56) 310 2939; Tel: +41 (56) 310 3569

We outline a linearized analysis of pulsed-source time-of-flight crystal analyzer spectrometers (CAS) based on scattered neutron analysis by crystal monochromators and intended for use in high-resolution quasielastic scattering and Brillouin scattering measurements. Spectrometers of this kind, often called "backscattering spectrometers," provide for high resolution measurements of excitations with typical energies in the range 1–100 µeV in both steady source and pulsed source applications. The analysis is fully general, treating three-dimensionally the geometric conditions for time focusing of the orientations of the source (moderator), sample, monochromator crystal and detector, considered as thin elements having large areas, and allows for the use of mosaic crystal monochromators. We report the results of VITESS Monte Carlo simulations, which verify the analytical focusing conditions for dispersionless excitations, reveal higher-order (than linear) contributions to the resolution widths, and provide absolute intensity estimates.

Motivation

We deal with pulsed-source crystal analyzer spectrometers, for example, IRIS, TOSCA, QENS, and the LAM instruments at ISIS, IPNS, and KENS, starting from a generalized concept of this class of machines.

The aim of the present analysis is to provide a basis for design of spectrometers of the highest possible resolution with the highest possible counting rates, meanwhile to reveal new flexibilities for the design.

The principle is to increase the areas of components and the range of wavelengths accepted, maintaining precise time resolution by "time-focusing." Variations of neutron flight path lengths and angles, correlated through the analyzer Bragg condition, compensate variations in the selected wavelengths.

The theory of time focusing of crystal analyzer spectrometers is the subject of a pair of recent papers.[1,2]

General principles of time-focusing

Fig. 1. illustrates the arrangement of components in an inverse geometry crystal analyzer spectrometer (CAS). Neutrons travel from the moderator to the sample, where they scatter; the analyzer crystal intercepts those in a range of solid angle and reflects those that satisfy the Bragg condition (for that path) into the detector.

Neutrons arrive at the detector at time t that depends on the path through the spectrometer

$$t = l_1(r_m, r_s)/v' + (l_2(r_s, r_x) + l_3(r_x, r_d))/v.$$

Neutrons reflected from the analyzer satisfy Bragg's law for that path,

$$\lambda = \lambda(r_s, r_x, r_d) = 2d \sin(\theta(r_s, r_x, r_d)).$$

We assume nondispersive (q-independent) excitations,

$$\varepsilon = (m/2)(v^2 - v'^2) = \frac{h^2}{2m}\left(1/\lambda'^2 - 1/\lambda^2\right).$$

Time-focusing requires that the time-of-arrival is constant, to first order independent of the deviations $\boldsymbol{\delta}_d$, etc., of the interaction positions r_m, r_s, r_x, r_d from their mean values R_m, etc.

We ignore the source pulse width (easily accounted for) and d-spacing variations in the crystals, which ultimately limit the resolution.

Linearized calculation

Considering the detector, for example, the interaction point is a small distance from the nominal center of the detector, so that the vector separating general points on the analyzer and the detector is $L_{xd} = R_d - R_x + \boldsymbol{\delta}_d - \boldsymbol{\delta}_x = L_{xd} + \boldsymbol{\delta}_d - \boldsymbol{\delta}_x$, where $\boldsymbol{\delta}_d = r_d - R_d$. Fig. 2 illustrates this case.

Time-focusing conditions

We merely outline the results, omitting, as the reader may expect, many pages of tedious algebra.[1]

The time-of-arrival at the detector (to first order in the $\boldsymbol{\delta}$'s) is

$$t = t_0 + (\boldsymbol{\delta}_m \text{ term}) + (\boldsymbol{\delta}_s \text{ term}) + (\boldsymbol{\delta}_x \text{ term}) + (\boldsymbol{\delta}_d \text{ term}).$$
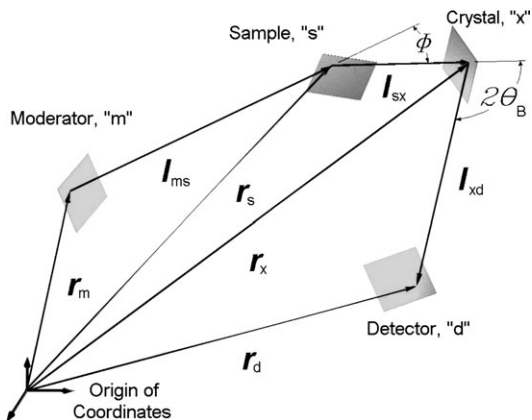
Four independent conditions arise when we require that these terms vanish to first order, for example, for the moderator,

$$(\boldsymbol{\delta}_m \text{ term}) = -\frac{1}{v_0}(\lambda'_0/\lambda_0)\hat{\boldsymbol{L}}_1 \cdot \boldsymbol{\delta}_m = 0,$$

which involves only $\boldsymbol{\delta}_m$.

For the detector,

$$(\boldsymbol{\delta}_d \text{ term}) = \frac{1}{v_0}\Bigg\{ \hat{\boldsymbol{L}}_3 - \frac{1}{4\sin^2\theta_0}[(\lambda'_0/\lambda_0)^3 L_1 + L_2 + L_3].$$

$$\times[-\cos 2\theta_0 \hat{\boldsymbol{L}}_3/L_3 + \hat{\boldsymbol{L}}_2/L_3] \Bigg\} \cdot \boldsymbol{\delta}_d = 0,$$

† Presented at the 7th International Conference on Quasi-elastic Neutron Scattering, Arcachon, France, September 1–4, 2004.

Fig. 1 Schematic diagram of the pulsed-source crystal analyzer. The lines represent a general path through the instrument. $l_{xd} = R_d - R_x + \delta_d - \delta_x = L_{xd} + \delta_d - \delta_x$.

which involves only δ_d. Similarly, for terms involving δ_s and δ_x. Variables δ_m, δ_s, δ_x, and δ_d are independently distributed, so that the variance of the arrival time distribution is the sum of the averages of squares of the four terms. Subscripts "0" and capital letters refer to nominal values, bolded characters are vectors, and circumflexes designate unit vectors.

The conditions are of the form of scalar products of a vector (in brackets {…}) and the deviations of the positions from their mean values, δ_d, *etc.* The equations (δ_d term) = 0, *etc.*, define planes on which the deviations δ_d, *etc.*, must lie (within thin components) for focusing.

The four relationships are four independent focusing conditions, which represent constraints on the geometry of the instrument. We summarize the four focusing conditions in the last section, below.

The results apply to mosaic as well as single-crystal analyzers and in the general case require use of off-cut crystals: reflecting plane not parallel to the cut surface.

Focusing conditions

The time-focusing conditions in the previous form are admittedly obscure, except the first, the moderator condition,

$$\frac{1}{v_0}(\lambda'/\lambda)\hat{L}_1 \cdot \delta_m = \frac{1}{v_0'}\hat{L}_1 \cdot \delta_m = 0,$$

which represents the intuitively satisfying requirement that the moderator surface be oriented perpendicular to the spectrometer incident beam direction:

$$\hat{L}_1 \cdot \delta_m = 0.$$

This condition relates to all energies and energy transfers because v_0' is finite, moreover, the condition applies even when
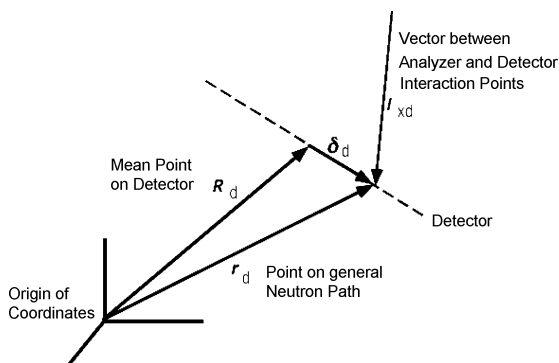
Fig. 2 The relationship between the mean point R_d on the detector, the general point r_d and the small deviation of the general point from the mean point, δ_d.
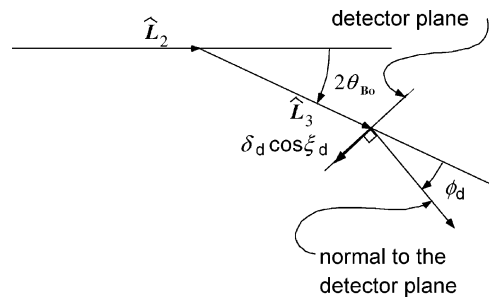
Fig. 3 The detector illustrated in the "analysis plane" defined by vectors L_2 and L_3. The focused detector orientation is perpendicular to the analysis plane.

a straight, parallel-sided guide directs neutrons from the source to the sample.

Ref. 2 provides two-dimensional diagrams that help to understand the contents of the focusing conditions. We illustrate in terms of the detector.

Detector focusing

The detector focusing condition requires that the detector plane lies perpendicular to the "analysis plane" defined by L_2 and L_3 and that the normal vector to the detector plane lies at a special angle ϕ_d^f with respect to the direction of neutrons reflected from the crystal:

$$\tan \phi_d^f = (L_3/2)[(\lambda_0'/\lambda_0)^3 L_1 + L_2 + L_3]\cot \theta_{B,0}.$$

Fig. 3 illustrates the geometry.

The form of the detector focusing condition illustrates two points valid for all crystal analyzer spectrometers:

(*i*) the detector focusing condition, and in general the resolution as affected by all of the components (except the moderator), depends on all the flight path lengths L_1, L_2 and L_3, so the "primary" and "secondary" spectrometers are interdependent;

(*ii*) focusing is possible for only one energy transfer, *i.e.*, only one (arbitrary) value of ε or (λ_o'/λ_o) in a given geometric arrangement; for example, for $\varepsilon = 0$ (elastic scattering), $(\lambda_o'/\lambda_o) = 1.0$, and focusing applies approximately for a narrow range around $\varepsilon = 0$, (quasi-elastic scattering).

Analyzer and sample focusing

The focusing conditions for the analyzer crystal and the sample are more involved, and we do not exhibit them here (but see ref. 2). However, we note some significant points:

(*i*) focusing of the analyzer crystal is possible for analyzer Bragg angles significantly different from 90° (backscattering); focusing of the analyzer requires either an off-cut crystal or equal sample-analyzer and analyzer-detector flight paths;

(*ii*) a particular focused orientation of the sample (within broad limits) admits the simultaneous focusing of a large range of scattering angles (analyzer arms).

Monte Carlo simulations

We have carried out Monte Carlo simulations of a crystal analyzer spectrometer using the powerful VITESS code.[3] We surveyed the time-of-arrival distributions as functions of the orientation of the components for a spectrometer with:

(*i*) $L_1 = 50$ m, $L_2 = 2$ m, $L_3 = 1.8$ m, $\Theta_{B,0} = 80°$;
(*ii*) analyzer reflectivity widths $\eta = 0.25°$, $0.5°$;
(*iii*) scattering angles 90° and 60°;
(*iv*) source 10×10 cm^2;
(*v*) sample, analyzer, and detector (5×5 cm$^2 \times 0.1$ mm).

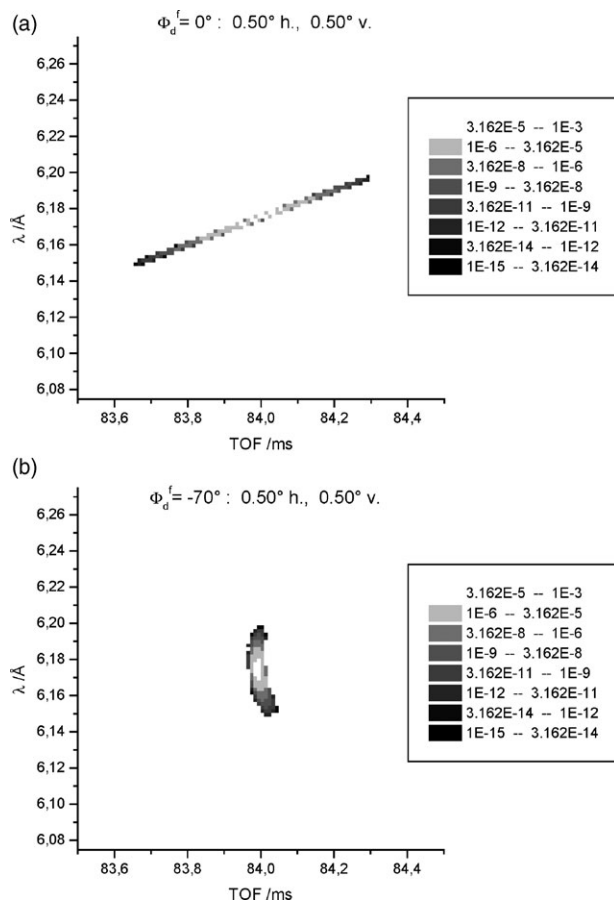The results[4] verify the focused orientations that the theory predicts, show the resolution contribution due to the higher-
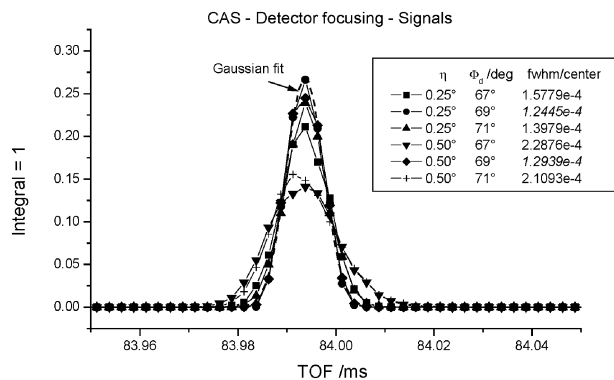
Fig. 4 Time-of-arrival distributions at the detector for a range of detector orientation angles around the focused value, $\phi_d^f = 69.2°$.

Fig. 6 Time distributions of neutrons arriving at the detector in the simulated prototype CAS for different sizes of analyzers.
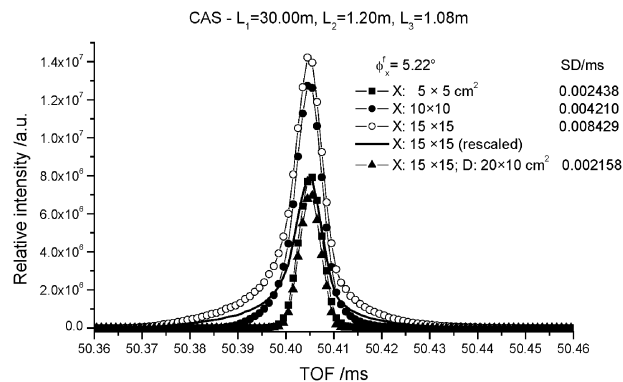
order terms in the time-of-arrival, provide detailed insight into the time-focusing effect, and also give the counting rate at the detector.

Focused, the relative FWHM of the time-of-arrival distribution is of the order of $\Delta t/t \approx 10^{-4}$, which remains finite because of nonlinear effects in the time-of-arrival, ignored in the linearized analysis but properly represented in the simulations. As an example, we show some detailed results for the detector in Fig. 4.

Plots of the detected neutron distribution as a joint function of wavelength and time reveal the nature of the focusing effect in Fig. 5a and 5b.

Fig. 5 (a) The distribution of wavelengths as a function of time-of-arrival at the detector, for an unfocused detector oriented normal to the direction of arriving neutrons, $\phi_d = 0°$ (perpendicular). (b) The distribution of wavelengths as a function of time-of-arrival at the detector, for a detector oriented close to the focused condition, $\phi_d = 70° \approx \phi_d^f = 69.2°$.

A prototype time-focused CAS

A recently completed upgrade of the general purpose powder diffractometer (GPPD) includes installation of a guide in the incident flight path. The GPPD beam emerges perpendicularly from the 100 K liquid CH_4 moderator. These modifications provide an opportunity to construct a testing station downstream at a distance of about 30 m from the moderator. We have conceived a test of a prototype time-focused CAS that we will locate there when time and resources allow.

We have simulated the performance of a 30 m prototype instrument such as we propose to install at IPNS. Fig. 6 shows the time-of-arrival distribution for different sizes of analyzers. Fig. 7 shows the wavelength distribution for different analyzer sizes.

Figs. 8 and 9 depict the distribution of wavelengths, times-of-arrival of neutrons at the detector and the 2D position distribution of neutrons arriving at the detector for a 5×5 cm^2 analyzer. The incident neutron flight path length assumed is $L_1 = 30$ m.

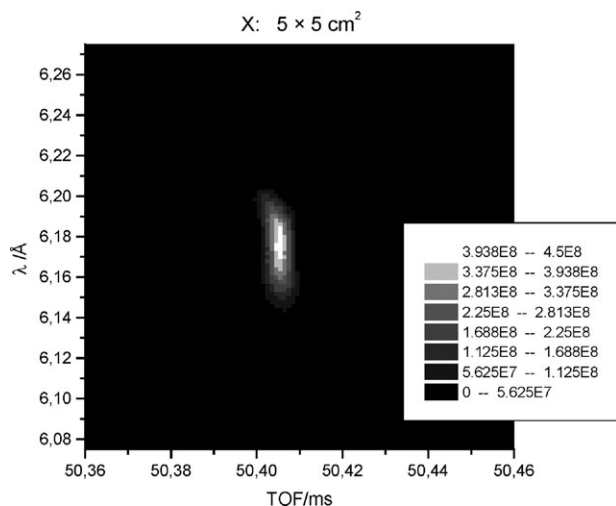### The emission-time distribution for the moderator of the prototype CAS

The width of the emission time distribution places a lower limit on the width of observed features of the scattering from the sample. The moderator serving the "F2" beam where the prototype CAS would be located consists of a decoupled, flowing liquid methane at 100 K, with poisoning 25 mm below the viewed surface. Fig. 10 shows the emission-time distribution for 5.7 Å neutrons.

Results and conclusions

Simulations of the 50 m and of the 30 m instruments verify the theoretical focusing conditions. The simulations of the
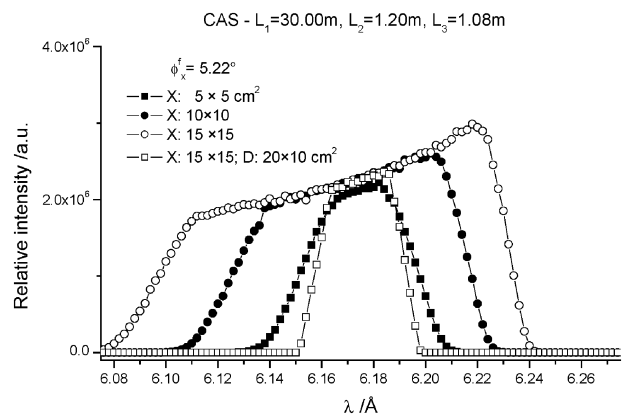
Fig. 7 The distributions of wavelengths accepted by the instrument as functions of the size of the analyzer crystal.

X: 5 × 5 cm²

Legend:
3.938E8 -- 4.5E8
3.375E8 -- 3.938E8
2.813E8 -- 3.375E8
2.25E8 -- 2.813E8
1.688E8 -- 2.25E8
1.125E8 -- 1.688E8
5.625E7 -- 1.125E8
0 -- 5.625E7

Fig. 8 The distribution of wavelengths and time-of-arrival for focused conditions.

30 m prototype for a 10×10 cm² analyzer show a standard deviation of the time-of-arrival distribution of 4.21 µs (FWHM = 9.9 µs). The time resolution due to the source pulse, based on the 15 µs 10–90% rise time of the emission time distribution (see Fig. 10), should be narrow enough to test the resolution of the time-focused spectrometer using modest deconvolution techniques.
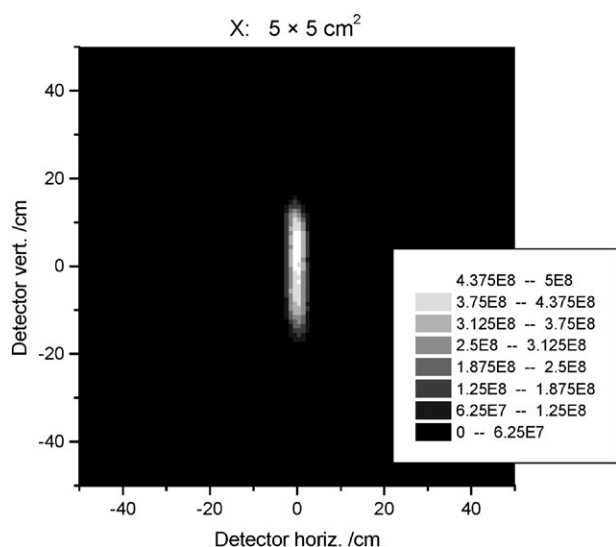
The simulations for the prototype 10×10 cm² analyzer show a time resolution relative to incident-path flight time

$$\Delta t/t = 2.11 \times 10^{-4}.$$

Because the selected wavelength, 6.17 Å, corresponds to an energy of 2.15 meV, the corresponding energy transfer resolution is $\Delta E = 0.90$ µeV, which should be adequate to show the potential of the time-focused instrument. The "raw" resolution based on the FWHM of the pulse would be approximately 3.9 µeV. There are excellent prospects for the prototype.

Further work

We obtained further results[5,6] on a realistic instrument example including a guide delivery system. We also checked how the energy resolution broadens at higher energy transfers when keeping the instrument focused in the conditions obtained for the elastic scattering. In the example instrument we have used

X: 5 × 5 cm²

Legend:
4.375E8 -- 5E8
3.75E8 -- 4.375E8
3.125E8 -- 3.75E8
2.5E8 -- 3.125E8
1.875E8 -- 2.5E8
1.25E8 -- 1.875E8
6.25E7 -- 1.25E8
0 -- 6.25E7

Fig. 9 The distribution of neutrons in the vertical and horizontal directions on the detector for focused conditions.

IPNS "F" Moderator, 100K CH4
2.53 meV, 5.686 Å

90%
15 µsec 10-90%
39 µsec FWHM
10%
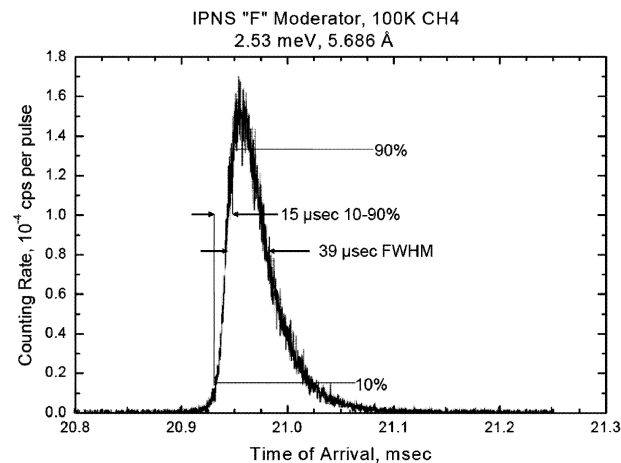
Fig. 10 The emission-time distribution of the IPNS "F" moderator for 5.7 Å neutrons. The time scale is offset according to the arrival time of the neutrons at 11.7 m distance. The 10–90% rise time is 15 µs. The FWHM is 39 µs.

the following parameters: moderator-sample distance $L_1 = 50.0$ m, sample analyzer distance $L_2 = 2.0$ m, analyzer-detector distance $L_3 = 1.8$ m, Bragg angle of the analyzers 80°. The scattering angle was 90°. The analyzer arm is rotated around the analyzer system vector W (see ref. 2) which was chosen vertical. As it can be seen in Fig. 11, the resolution broadens only slightly up to 0.5 meV transfer. The resolution FWHM becomes 21 µeV at 2 meV transfer. Further analysis will be done to compare to a backscattering instrument (analyzer Bragg angle near 90°) having similar flight paths and component sizes.

We have also carried out a general-level analysis of a crystal analyzer spectrometer for the case of isotropic, linearly dispersive excitations (Brillouin scattering). The results are similar in form to the summary focusing conditions cited next, but considerably more complicated. A report is in preparation.[7]

A final note: application to direct geometry instruments

Our results apply as stated for "inverse geometry" spectrometers, that is, ones in which a crystal monochromator determines the final energy while time-of-flight across the incident flight path determines the incident energy and thus the energy transfer.

However, the same results apply for "direct geometry," requiring only exchanging (m,s,x,d) → (d,s,x,m), (1,2,3) → (3,2,1), the reversal of the primed and unprimed variables, and of the sign of the energy transfer.

energy transfer	SD/meV
0	0.00684
0.05	0.00689
0.5	0.00738
1.0	0.00815
2.0	0.01035
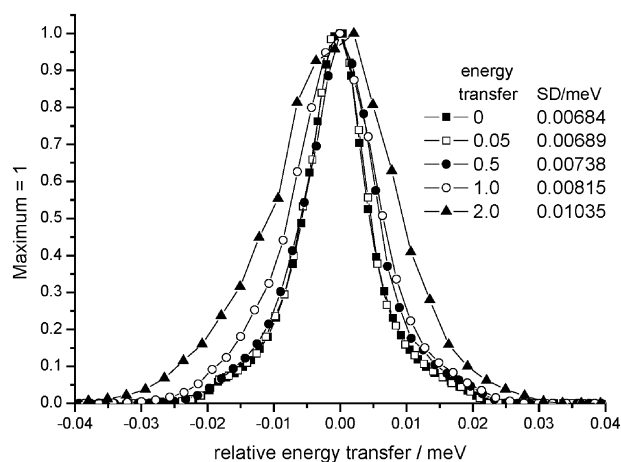
Fig. 11 The change in energy resolution at various energy transfers keeping the same focusing condition obtained for elastic scattering.

Summary of time-focusing conditions

Here we collect the time-focusing conditions for all the components.

For the moderator,

$$(\boldsymbol{\delta}_{\mathrm{m}}\text{ term}) = -\frac{1}{v_0}(\lambda'_0/\lambda_0)\hat{\boldsymbol{L}}_1 \cdot \boldsymbol{\delta}_{\mathrm{m}} = 0$$

For the sample,

$$(\boldsymbol{\delta}_{\mathrm{s}}\text{ term}) = \frac{1}{v_0}\left\{ [(\lambda'_0/\lambda_0)\hat{\boldsymbol{L}}_1 - \hat{\boldsymbol{L}}_2] - \frac{1}{4\sin^2\theta_0}[(\lambda'_0/\lambda_0)^3 L_1 \right.$$
$$\left. + L_2 + L_3] \times [\cos 2\theta_0 \hat{\boldsymbol{L}}_2/L_2 - \hat{\boldsymbol{L}}_3/L_2] \right\} \cdot \boldsymbol{\delta}_{\mathrm{s}} = 0$$

For the analyzer,

$$(\boldsymbol{\delta}_{\mathrm{x}}\text{ term}) = \frac{1}{v_0}\left\{ [\hat{\boldsymbol{L}}_2 - \hat{\boldsymbol{L}}_3] - \frac{1}{4\sin^2\theta_{B,0}}[(\lambda'_0/\lambda_0)^3 L_1 + L_2 + L_3] \right.$$
$$\left. \times [-(\cos 2\theta_{B,0})[(\hat{\boldsymbol{L}}_2/L_2 - \hat{\boldsymbol{L}}_3/L_3) - \hat{\boldsymbol{L}}_2/L_3 - \hat{\boldsymbol{L}}_3/L_2] \right\} \cdot \boldsymbol{\delta}_{\mathrm{x}},$$

For the detector,

$$(\boldsymbol{\delta}_{\mathrm{d}}\text{ term}) = \frac{1}{v_0}\left\{ \hat{\boldsymbol{L}}_3 - \frac{1}{4\sin^2\theta_0}[(\lambda'_0/\lambda_0)^3 L_1 + L_2 + L_3] \right.$$
$$\left. \times [-\cos 2\theta_0 \hat{\boldsymbol{L}}_3/L_3 + \hat{\boldsymbol{L}}_2/L_3] \right\} \cdot \boldsymbol{\delta}_{\mathrm{d}} = 0$$

Ref. 2 provides geometrical interpretations of these conditions.

References

1 J. M. Carpenter, *Nucl. Instrum. Methods Phys. Res., Sect. A*, 2002, **483**, 774.
2 J. M. Carpenter, E. B. Iverson and D. F. R. Mildner, *Nucl. Instrum. Methods Phys. Res., Sect. A*, 2002, **483**, 784.
3 G. Zsigmond, K. Lieutenant and F. Mezei, *Neutron News*, 2002, **13/4**, 11, see also VITESS web-site http://www.hmi.de/projects/ess/vitess/.
4 G. Zsigmond, J. M. Carpenter and F. Mezei, *SPIE Proc.*, 2002, **4785**, 91.
5 G. Zsigmond and J. M. Carpenter, *Nucl. Instrum. Methods Phys. Res., Sect. A*, 2005, accepted.
6 G. Zsigmond, K. Lieutenant, S. Manoshin, H. N. Bordalo, J. D. M. Champion, J. Peters, J. M. Carpenter and F. Mezei, *Nucl. Instrum. Methods Phys. Res., Sect. A*, 2004, **529**, 218.
7 N. L. Wilson, J. M. Carpenter and C. J. Benmore, in preparation.